RSC Advances

PAPER

View Article Online
View Journal | View Issue

Cite this: *RSC Adv.*, 2025, **15**, 19318

New strategy for optimizing the microstructure and giant dielectric properties of TiO_2 *via* acceptor/donor ratio tuning†

Wattana Tuichai,[a] Jurimart Wongsricha,[a] Nutthakritta Phromviyo,[b] Bundit Putasaeng,[c] Supamas Danwittayakul,[c] Pornjuk Srepusharawoot[ab] and Prasit Thongbai*[ab]

In this study, we investigated how the acceptor/donor doping ratio influences the microstructure and giant dielectric behavior of co-substituted TiO_2 ceramics. $Sc_xTa_{0.025}Ti_{0.975-x}O_2$ ceramics, with Sc^{3+}/Ta^{5+} ratios of 0.4, 0.8, 1.0, and 2.0, were synthesized *via* solid-state reactions. All samples crystallized into dense rutile TiO_2, and Raman spectroscopy revealed that increasing the Sc^{3+}/Ta^{5+} ratio promotes the formation of oxygen vacancies, leading to larger average grain sizes. The dielectric constant (ε') decreased significantly with higher Sc^{3+}/Ta^{5+} ratios, and no giant dielectric response was observed for ratios above 1.0. Notably, samples with Sc^{3+}/Ta^{5+} ratios of 0.4 and 0.8 achieved ε' values of 5.9×10^4 and 4.8×10^4, respectively, alongside low loss tangents ($\tan\delta$) of 0.024 and 0.043 at 1 kHz and 25 °C. These ceramics also exhibited excellent temperature stability, with their ε' values varying by less than ±15% from −60 to 210 °C—sufficient for X9R capacitor applications. Impedance spectroscopy and nonlinear electrical measurements revealed that the enhanced dielectric performance arises primarily from interfacial polarization effects due to insulating grain boundaries and conductive grains, as further confirmed by X-ray photoelectron spectroscopy. Interestingly, the optimal dielectric properties, commonly reported at an acceptor/donor ratio of 1.0 in other co-doped systems, were not observed in this study. These findings challenge the conventional assumption that a 1 : 1 acceptor/donor ratio is universally optimal for co-doped TiO_2 ceramics. This work provides a new strategy for enhancing dielectric performance by adjusting the doping ratio in systems dominated by extrinsic mechanisms such as IBLC.

Received 23rd March 2025
Accepted 29th May 2025

DOI: 10.1039/d5ra02034d

rsc.li/rsc-advances

1. Introduction

Giant dielectric oxides with dielectric permittivities (ε') exceeding 10^3 have garnered significant interest due to their potential applications in ceramic capacitors (CCs) and high-energy-density storage (HEDS) devices.[1,2] Many non-ferroelectric complex and simple oxides exhibit remarkably high dielectric properties without undergoing ferroelectric phase transitions.[3–8] Several mechanisms have been proposed to explain these giant dielectric phenomena, including the internal barrier layer capacitor (IBLC) model,[4–6] surface barrier layer capacitor (SBLC) model,[9] polaronic stacking fault defects,[10] small polaron hopping,[11] and the non-ohmic sample-electrode (SE) contact model.[12,13] Despite significant progress, the temperature stability of ε' remains a key challenge for their practical implementation in CCs and HEDS applications.

Titanium dioxide (TiO_2) ceramics have attracted widespread attention due to their excellent dielectric properties, structural versatility (anatase, rutile, and brookite phases), and broad applicability in areas such as energy storage, environmental science, and medicine.[7,8] Among these polymorphs, rutile TiO_2 stands out due to its high ε' and relatively low loss tangent ($\tan\delta$), making it a promising material for dielectric and capacitor applications.

Recent research has highlighted the remarkable dielectric performance of co-substituted rutile TiO_2 materials, which exhibit very high ε' and low $\tan\delta$ over a broad temperature range, making them promising candidates for high-performance CCs and HEDS applications. For instance, In^{3+}, Nb^{5+} co-doped TiO_2 (InNb-TO) ceramics have demonstrated $\varepsilon' \approx 64\,000$ and $\tan\delta < 0.025$.[8] This behavior is primarily attributed to the electron pinned defect-dipole (EPDD) model, where In^{3+} doping induces oxygen vacancy ($V_O^{\cdot\cdot}$)-related complex defects that confine the free electrons introduced by Nb^{5+} doping.

Understanding the origins of the giant dielectric response and the roles of dopants in TiO_2-based ceramics remains

[a]*Giant Dielectric and Computational Design Research Group (GD-CDR), Department of Physics, Faculty of Science, Khon Kaen University, Khon Kaen 40002, Thailand. E-mail: pthongbai@kku.ac.th; Fax: +66 43 202374; Tel: +66 84 4190266*

[b]*Institute of Nanomaterials Research and Innovation for Energy (IN-RIE), Khon Kaen University, Khon Kaen 40002, Thailand*

[c]*National Metal and Materials Technology Center, 114 Thailand Science Park, Paholyothin Road, Klong 1, Klong Luang, Pathumthani 12120, Thailand*

† Electronic supplementary information (ESI) available. See DOI: https://doi.org/10.1039/d5ra02034d

a critical research topic. While the EPDD model is widely recognized as a key mechanism in co-doped TiO_2, alternative mechanisms such as IBLC and SBLC have also been proposed.[9,14–17] Despite the diversity of these models, high ε', excellent temperature stability, and low dielectric loss are crucial properties for practical applications. Recent broadband dielectric spectroscopy studies have confirmed that multiple dielectric responses can achieve $\varepsilon' > 10^3$, further emphasizing the importance of elucidating the underlying mechanisms.[18,19]

To enhance dielectric performance, researchers have explored a variety of dopant combinations in co-doped TiO_2, including (Gd^{3+}, Nb^{5+}),[20] (Cu^{2+}, Nb^{5+}),[21] (In^{3+}, Ta^{5+}),[22] (Ag^{+}, Ta^{5+}),[23] (Tm^{3+}, Nb^{5+}),[24] (Eu^{3+}, Nb^{5+}),[25] (Pr^{3+}, Ta^{5+}),[26] (Zr^{4+}, Ta^{5+}),[27] (Ga^{3+}, Nb^{5+}),[11] (Al^{3+}, Nb^{5+}),[28] (Zn^{2+}, W^{6+}),[29] (Ag^{+}, Mo^{6+}),[30] and (Ca^{2+}, Ta^{5+}).[31] In most of these studies, trivalent and pentavalent dopants were introduced at equal concentrations (+3/+5 ratio = 1), based on the assumption that donor dopants primarily enhance the dielectric response, while acceptor dopants regulate tan δ. However, recent findings suggest that this assumption may be oversimplified, and the interactions between donor and acceptor dopants are more complex than previously thought.

For example, in aluminum–niobium co-doped TiO_2 (InAl-TO) ceramics,[28] Nb^{5+} doping was expected to increase ε' by generating free electrons. In other words, a reduction in ε' should be attributed solely to the decrease in Nb^{5+}, while Al^{3+} doping is expected to primarily regulate tan δ. However, contrary to these expectations, ε' was found to decrease with increasing Al^{3+} concentration. This suggests that ε' is influenced not only by Nb^{5+} but also by the presence of Al^{3+}. The unexpected decline in ε' was attributed to Al^{3+}, which primarily induces $V_O^{\cdot\cdot}$ and typically does not significantly alter ε' or the concentration of free electrons. However, Al^{3+} appears to interact with Nb^{5+}, indicating a possible self–charge compensation mechanism between these ions. Unfortunately, this interaction remains largely unexplored. In practice, partial self-charge compensation between trivalent (+3) and pentavalent (+5) ions may occur without the formation of additional point defects, implying that an equal acceptor/donor ratio may not always be optimal. To achieve better dielectric performance, acceptor dopants should primarily reduce dielectric loss while minimizing any perturbation to ε'. This leads to an important hypothesis: the acceptor/donor ratio should be lower than 1.0 rather than strictly equal to 1.0.

Many previous studies have assumed that an acceptor/donor ratio of 1.0 is necessary for maximizing dielectric properties in co-doped TiO_2, particularly in systems where EPDD is the dominant mechanism, such as InNb-TO.[8] In such cases, In^{3+} and Nb^{5+} work synergistically to create complex defect structures that enhance the dielectric response. However, in co-doped TiO_2 systems where giant dielectric properties arise primarily from extrinsic mechanisms such as IBLC and SBLC—rather than EPDD—the situation may be entirely different. This is evident in Sc^{3+}, Ta^{5+} co-doped TiO_2 (ScTa-TO), where Sc^{3+} (acceptor) promotes the formation of insulating grain boundaries, while Ta^{5+} (donor) enhances conductivity in the grain interiors.[9] Unlike the InNb-TO system, where both dopants cooperate to form a defect complex, Sc^{3+} and Ta^{5+} do not work together in the same way. This suggests that the commonly assumed +3/+5 ratio of 1.0 may not always yield optimal dielectric performance in TiO_2 ceramics. These findings indicate that the optimal acceptor/donor ratio is closely related to the predominant dielectric mechanism. In systems governed by EPDD, such as InNb-TO or In^{3+}, Ta^{5+} co-doped TiO_2 (InTa-TiO_2),[8,32] a 1 : 1 ratio is theoretically expected to be optimal for forming electron–trapping complex defects that enhance the dielectric response. In contrast, for systems dominated by the IBLC mechanism, such as ScTa-TiO, a reduced acceptor concentration may help maintain free electron generation and strengthen interfacial polarization. This work, therefore, introduces a design strategy that can be adapted to other extrinsically driven dielectric systems. The insight gained here offers a new conceptual basis for tailoring co-doped TiO_2 ceramics by adjusting the acceptor/donor ratio in accordance with the underlying dielectric mechanism.

Our previous study investigated ScTa-TiO ceramics with selected Sc^{3+} concentrations (1, 2.5, and 5%), focusing primarily on humidity sensitivity.[33] It was found that the ε' value for the sample with a Sc^{3+}/Ta^{5+} ratio of 1.0 remained below 10^4, even when sintered at 1500 °C. In contrast, the sample with a Sc^{3+}/Ta^{5+} ratio of 0.4 exhibited a much higher ε' ($\sim 10^5$), but this was accompanied by a relatively high tan δ. These observations suggested that the optimal dielectric behavior might not occur at the conventional 1 : 1 ratio, yet the underlying origin and systematic relationship between microstructure and dielectric properties were not clarified.

The present work expands upon those findings by systematically investigating the influence of the Sc^{3+}/Ta^{5+} ratio over a broader and finer compositional range (0.4, 0.8, 1.0, 1.2, 1.6, and 2.0), under identical processing conditions. By decoupling the effects of different mechanisms, this study seeks to establish the correlation between doping ratio, microstructure, and dielectric properties, and to determine whether the optimal performance truly aligns with a 1 : 1 acceptor/donor ratio. This research introduces a new strategy for tailoring co-doped TiO_2 ceramics, especially in systems dominated by IBLC effects. Through targeted control of grain boundary characteristics and dopant interactions, the work aims to provide guiding principles for developing high-performance dielectric materials with excellent temperature stability and low tan δ.

2. Experimental details

The ScTa-TO ceramics were designed with various acceptor/donor ratios of 0.4, 0.8, 1.0, 1.2, 1.6 and 2.0. Correspondingly, the $Sc_xTa_{0.025}Ti_{0.975-x}O_2$ ceramics, where Sc^{3+}/Ta^{5+} ratios of 0.4, 0.8, 1.0, and 2.0, were synthesized using a conventional solid-state reaction (SSR) method. The preparation steps for obtaining the mixed powders are detailed in previous work.[9] The mixed powders were pressed into pellets with a diameter of 9.5 mm and a thickness of 1.5 mm using uniaxial compression at approximately 210 MPa, without the use of a binder. The ceramic samples were then sintered at 1400 °C for 5 h with a heating rate of 2 °C min^{-1}, followed by natural furnace cooling

to room temperature. The sintered ceramics with the specified acceptor/donor ratios were referred to as (Sc/Ta)0.4, (Sc/Ta)0.8, (Sc/Ta)1.0, (Sc/Ta)1.2, (Sc/Ta)1.6, and (Sc/Ta)2.0, respectively. The densities of the sintered samples were measured using the Archimedes method.

To characterize the sintered ScTa-TO specimens, a comprehensive suite of analytical techniques was employed, including UV-Vis Raman spectroscopy, scanning electron microscopy (SEM), X-ray diffraction (XRD), field-emission scanning electron microscopy (FE-SEM) with energy-dispersive X-ray analysis (EDS), and X-ray photoelectron spectroscopy (XPS). Detailed descriptions of these techniques can be found in our previous publication.[9]

For the dielectric and nonlinear electrical measurements, both surfaces of the sintered samples were polished, cleaned, and dried at 100 °C for 2 h. Silver (Ag) paint was then applied to form electrodes, followed by heating at 600 °C for 0.5 h to ensure proper adhesion. The dielectric and electrical properties were measured using a KEYSIGHT E4990A Impedance Analyzer with an oscillation voltage of 0.5 V. Dielectric measurements were conducted over a frequency range of 40 Hz to 1 MHz and a temperature range of −180 to 200 °C. The nonlinear current density–electric field (J–E) characteristics were evaluated at ~25 °C using a Keithley Model 247 high-voltage measurement unit. The breakdown field (E_b) was determined at J = 1 mA cm^{-2}, while the nonlinear coefficient (α) was calculated over the J range of 1–10 mA cm^{-2}.

3. Results and discussion

The XRD patterns of ScTa-TO ceramics, with Sc^{3+}/Ta^{5+} ratios of 0.4, 0.8, 1.0, 1.2, 1.6, and 2.0, are presented in Fig. 1. The diffractograms reveal distinct peaks corresponding to the rutile TiO_2 phase (JCPDS card no. 21-1276),[19,20,24,27] indicating that all compositions retain the rutile structure after doping with Sc^{3+} and Ta^{5+}. The peaks at 2θ positions ~27.4, 36.1, 41.2, 54.3, and 69.1° are indexed to the (110), (101), (200), (211), and (301) planes,[34] respectively, confirming the maintenance of the tetragonal rutile phase across all doping levels. No secondary phases or impurity peaks were detected, suggesting incorporation of Ta^{5+} and Sc^{3+} ions into the rutile lattice without forming new phases. However, while no Sc-related secondary phase is detectable in the XRD pattern of the (Sc/Ta)2.0 ceramic, due to the resolution limitations of the technique, segregation of Sc-related phases was observed in the SEM mapping, which will be discussed further in the microstructure analysis section.

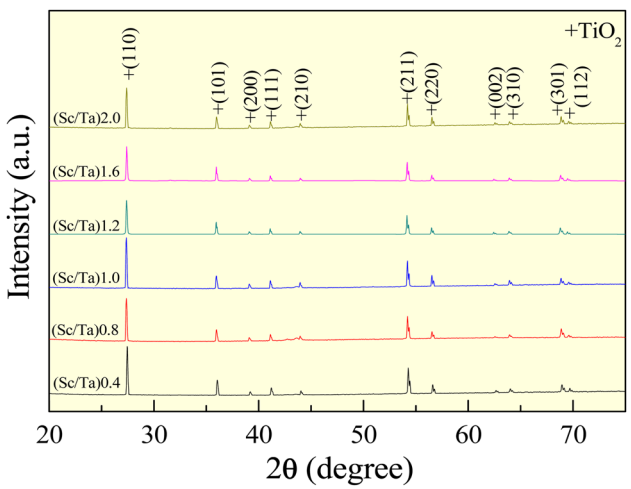

Fig. 1 XRD patterns of ScTa-TO ceramics with Sc^{3+}/Ta^{5+} ratios of 0.4, 0.8, 1.0, 1.2, 1.6, and 2.0.

Table 1 Lattice parameters, Raman peaks, mean grain size, and density of TiO_2 and ScTa-TO ceramics with Sc^{3+}/Ta^{5+} ratios of 0.4, 0.8, 1.0, and 2.0

Sample	TiO_2	(Sc/Ta)0.4	(Sc/Ta)0.8	(Sc/Ta)1.0	(Sc/Ta)2.0
Rietveld refinement					
$a = b$ (Å)	4.593	4.597	4.596	4.596	4.598
c (Å)	2.961	2.964	2.964	2.965	2.966
c/a	0.644(7)	0.644(8)	0.644(9)	0.645(1)	0.645(1)
V (Å)^3	62.475	62.631	62.597	62.620	62.708
R_{exp} (%)	4.209	5.834	6.603	6.072	6.071
R_p (%)	3.266	4.203	4.608	3.968	4.234
R_{wp} (%)	4.839	6.910	8.076	7.283	6.876
χ^2	1.321	1.403	1.496	1.439	1.283
Raman shift					
E_g	447.9	446.4	446.4	445.4	445.1
A_{1g}	611.3	611.8	611.5	610.9	609.9
Microstructure					
ρ (g cm^{-3})	4.13	4.06	4.11	4.14	3.92
$\bar{G}$ (μm)	41.7 ± 14.3	6.1 ± 1.8	7.9 ± 2.2	17.0 ± 6.3	17.7 ± 7.3

The lattice parameters (a and c values) derived from Rietveld refinements of the XRD patterns are summarized in Table 1 and Table S1 (ESI),† with the full refinement details provided in Fig. S1 (ESI).† The quality of the Rietveld refinements is reflected in the reliability factors R_{exp}, R_p, R_{wp}, and χ^2, with all samples exhibiting χ^2 values below 1.5, indicating robust structural models. The lattice expansion observed in the ScTa-TO ceramics compared to undoped TiO_2 is attributed to the substitution of smaller Ti^{4+} ions (ionic radius: 0.605 Å) by larger Sc^{3+} (0.745 Å) and Ta^{5+} (0.64 Å) ions.[9] Interestingly, while the lattice parameters exhibit some changes with increasing Sc^{3+} content, the c/a ratio remains relatively stable. This contrasts with what is observed in InNb-TO ceramics, where a significant increase in the c/a ratio with increasing In^{3+} content suggests preferential In^{3+} location along the c-axis, leading to the formation of extended planar defects (EPDDs).[8] The absence of a significant change in the c/a ratio in the ScTa-TO ceramics, as indicated by XRD analysis, suggests that EPDDs do not preferentially form in these materials, aligning with theoretical predictions from previous work.[9]

The microstructure of the ScTa-TO ceramics, where Sc^{3+}/Ta^{5+} ratios of 0.4, 0.8, 1.0, and 2.0, was analyzed using SEM, and the resulting images are presented in Fig. 2. As observed, the grain sizes ($\bar{G}$) of the ceramics exhibit noticeable changes with varying Sc^{3+} concentrations, as summarized in Table 1. Generally, as the Sc^{3+} concentration increases, the $\bar{G}$ appears to increase as well,

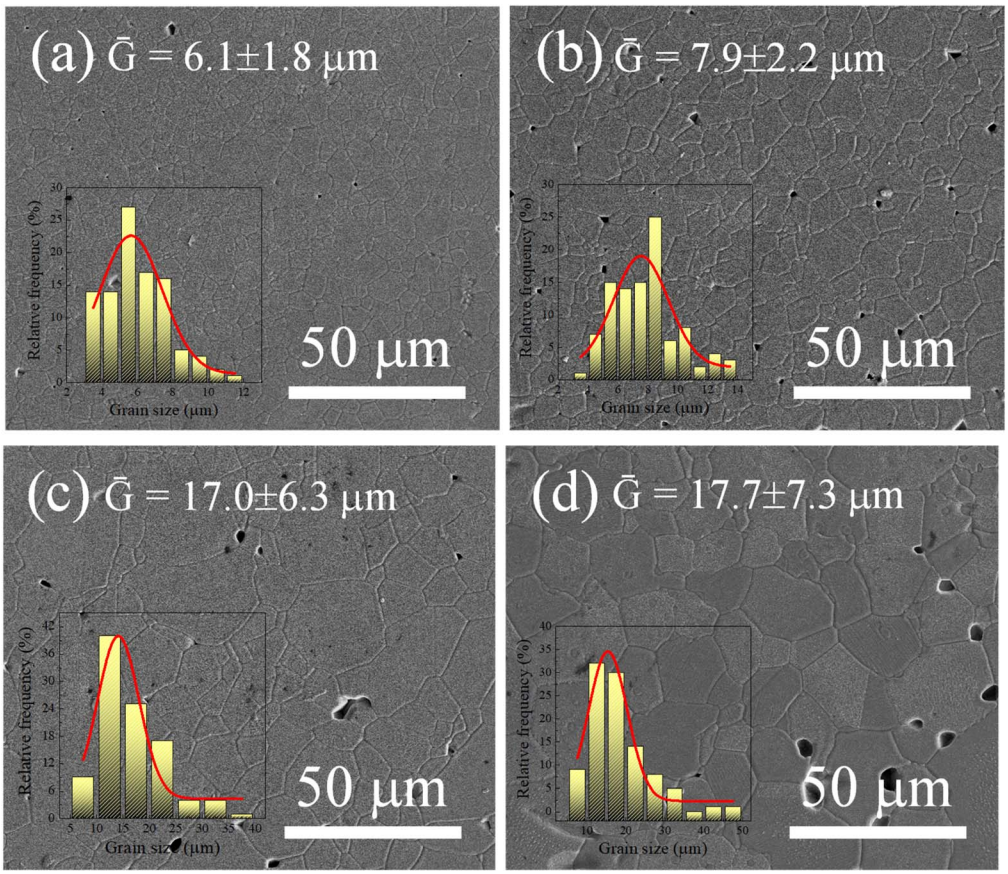

Fig. 2 SEM images of ScTa-TO ceramics with Sc^{3+}/Ta^{5+} ratios of (a) 0.4, (b) 0.8, (c) 1.0, and (d) 2.0.

particularly when comparing the ceramics with Sc^{3+}/Ta^{5+} ratios = 0.4 and 2.0. The $\bar{G}$ values in the ScTa-TO ceramics are larger than those of 2.5%Ta^{5+}-doped TiO_2 alone (~8.3 μm) at the sintering temperature of 1400 °C for 4 h, as reported in previous work,[16] suggesting that the function of Sc^{3+} in the co-doped system is similar to that of Ga^{3+} in promoting grain growth. In the 2.5%Ta^{5+}-doped TiO_2 ceramic, Ta^{5+} acts as a grain growth inhibitor, leading to smaller grain sizes by reducing grain boundary mobility due to its segregation at grain boundaries.[35] In contrast, both Ga^{3+} and Sc^{3+} are known to produce $V_O^{\cdot\cdot}$ during the sintering process, which enhances grain boundary mobility and promotes grain growth *via* the increase in diffusion rate of oxygen ions and $V_O^{\cdot\cdot}$.[9,16] In the case of ScTa-TO ceramics, it is evident that Sc^{3+} counteracts the grain size reduction caused by Ta^{5+}, resulting in larger grains, particularly in the higher Sc^{3+} concentration samples, *e.g.*, (Sc/Ta)2.0 ceramic. The micrographs of the (Sc/Ta)1.0 ceramic (Fig. 2c) show relatively uniform grain distribution, and a slightly increased grain size compared to the (Sc/Ta)0.4 ceramic (Fig. 2a). However, the (Sc/Ta)2.0 ceramic (Fig. 2d) displays the most significant grain growth, with larger grains and more pronounced grain boundary mobility. The (Sc/Ta)2.0 ceramic show the largest pore size and large number of pores, corresponding to its lowest density. This behavior is consistent with the function of Sc^{3+} as a promoter of grain boundary diffusion, facilitating the migration of grain boundaries and leading to enhanced grain growth. Additionally, future studies could explore how variations in grain size, along with the electrical properties of the grains and grain boundaries, affect the material's dielectric properties, as grain size is a critical factor in determining overall dielectric behavior.

The SEM-mapping images of the ScTa-TO ceramics, as shown in Fig. 3 and 4, illustrate the elemental distribution for (Sc/Ta)1.0 and (Sc/Ta)2.0 ceramics. In the (Sc/Ta)1.0 ceramic (Fig. 3), the mapping images indicate that Ti, O, Ta, and Sc are homogeneously distributed throughout the microstructure. Similar result is also observed in the (Sc/Ta)0.4 and (Sc/Ta)0.8 ceramics, as shown in Fig. S2 and S3,† respectively. This uniform dispersion suggests that the dopants are well-incorporated into the TiO_2 matrix at this doping level. Conversely, the (Sc/Ta)2.0 ceramic (Fig. 4) reveals notable segregation of Sc-rich phase particles, particularly evidenced by the scattered blue regions in the Sc mapping image, indicating the formation of secondary phases at higher doping concentrations. This observation is consistent with the increasing Sc^{3+} content detected by the EDS spectra, which show a progressive rise in the Sc percentage as the Sc^{3+} doping concentration increases. These findings suggest that the solubility limit of Sc^{3+} in the TiO_2 matrix is exceeded in the (Sc/Ta)2.0 ceramic, leading to the observed phase segregation.

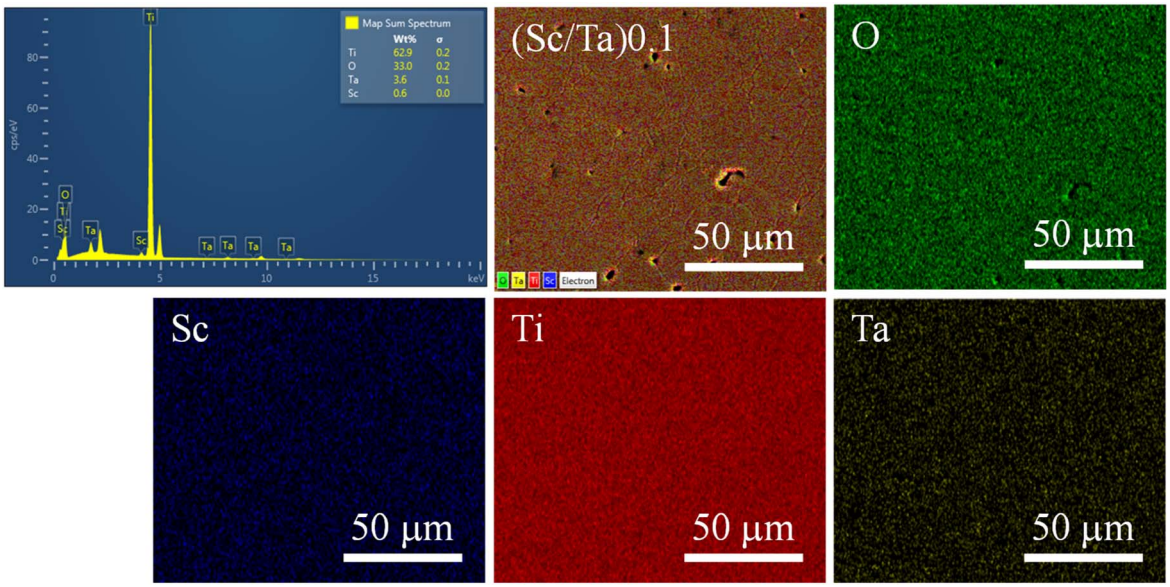

Fig. 3 EDS spectrum and SEM-mapping images of (Sc/Ta)1.0 ceramic.

Fig. 5 presents the Raman spectra of ScTa-TO ceramics Sc^{3+}/Ta^{5+} ratios of 0.4, 0.8, 1.0, and 2.0 compared to pure TiO_2. The spectra reveal the characteristic E_g and A_{1g} modes of rutile TiO_2, which correspond to oxygen vibrations within the lattice.[24,36–38] A noticeable shift in both Raman modes occurs as the Sc^{3+} concentration increases, indicating the impact of Sc^{3+} substitution on the TiO_2 structure. The E_g mode is detected at 446.4 cm^{-1} for both the (Sc/Ta)0.4 and (Sc/Ta)0.8 ceramics, and it downshifts slightly to 445.4 cm^{-1} and 445.1 cm^{-1} for the (Sc/Ta)1.0 and (Sc/Ta)2.0 ceramics, respectively. This consistent downshift of the E_g mode is attributed to the formation of $V_O^{\cdot\cdot}$, which tend to slightly increase as the Sc^{3+} concentration rises. Sc^{3+} substitution into the TiO_2 lattice requires charge compensation, typically achieved by generating $V_O^{\cdot\cdot}$.[38] The observed shift in the E_g mode of ScTa-TO ceramics compared to pure TiO_2 aligns well with previously reported studies.[9] For example, Parker *et al.* observed a shift in the E_g mode from 447 to 443 cm^{-1} as the [O]/[Ti] decreased from 2.0 to 1.99.[39] The presence of $V_O^{\cdot\cdot}$ due to Sc^{3+} doping ions can be explained by the following charge compensation reaction[9,15]

$$Sc_2O_3 \xrightarrow{2TiO_2} 2Sc_{Ti}^{'} + V_o^{\cdot\cdot} + 3O_O \quad (1)$$

The shift in the E_g peak position corroborates the increase in $V_O^{\cdot\cdot}$ concentration, as predicted by eqn (1). However, it should be noted that a Sc-rich second phase was observed in the (Sc/Ta)2.0

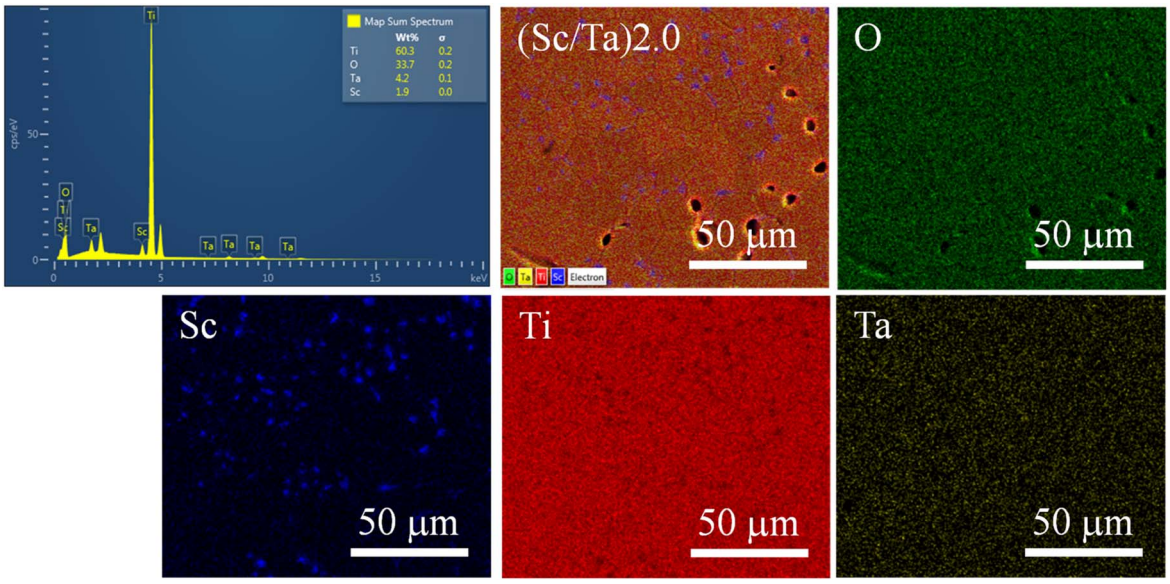

Fig. 4 EDS spectrum and SEM-mapping images of (Sc/Ta)2.0 ceramic.

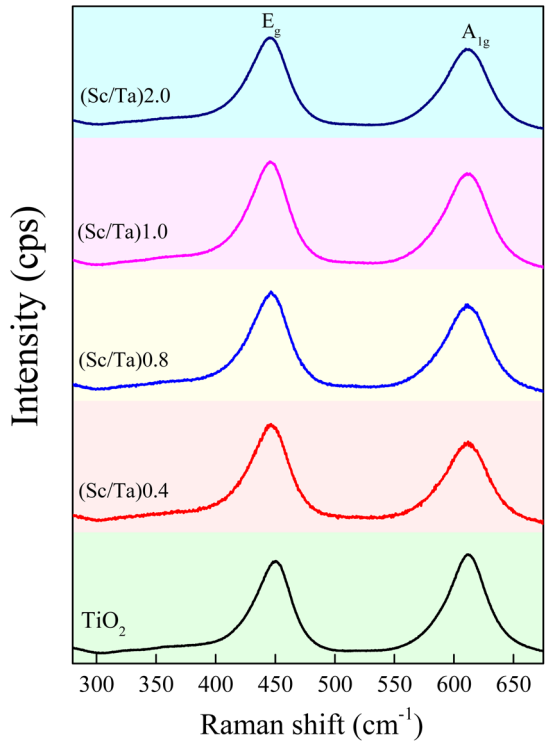

Fig. 5 Raman spectra of TiO_2 and ScTa-TO ceramics with Sc^{3+}/Ta^{5+} ratios of 0.4, 0.8, 1.0, and 2.0.

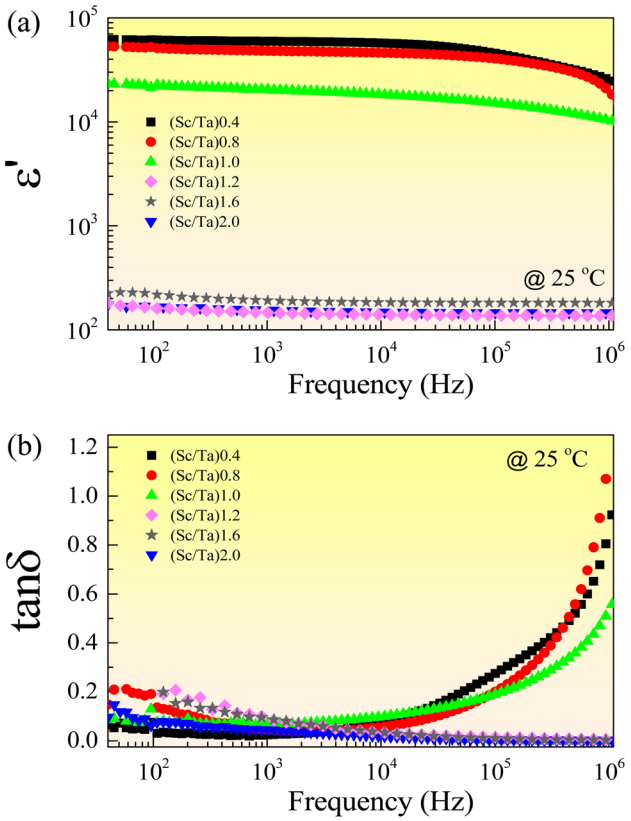

Fig. 6 Frequency dependence of (a) ε' and (b) tan δ at 25 °C for ScTa-TO ceramics with Sc^{3+}/Ta^{5+} ratios of 0.4, 0.8, 1.0, 1.2, 1.6, and 2.0.

ceramic (Fig. 4). This suggests that the solubility limit of Sc^{3+} in the ScTa-TO ceramics is slightly higher than 2.5%. Beyond this point, additional Sc^{3+} substitution may not be observed, and no further creation of $V_O^{\cdot\cdot}$ occurs. This may explain the relatively small difference in the E_g peak position between the (Sc/Ta)1.0 and (Sc/Ta)2.0 ceramics.

The A_{1g} mode also shows a gradual downshift, from 611.8 cm^{-1} in the (Sc/Ta)0.4 ceramic to 610.9 cm^{-1} for the (Sc/Ta)1.0 ceramic, and finally to 609.9 cm^{-1} in the (Sc/Ta)2.0 ceramic. This shift in the A_{1g} mode can be attributed to O–Ti–O bond vibrations, which may be altered by local distortions in the lattice caused by the substitution of Ti^{4+} with Sc^{3+} and Ta^{5+}. While the A_{1g} mode is less sensitive to $V_O^{\cdot\cdot}$ than the E_g mode, the consistent downshift indicates that the Ta^{5+} and Sc^{3+} substitution modifies the bonding environment within the lattice. The observed shifts in both the E_g and A_{1g} modes suggest that increasing Sc^{3+} concentration results in the introduction of more $V_O^{\cdot\cdot}$ concentrations, confirming the presence of an oxygen-deficient environment. These vacancies are likely responsible for the enlarged grain size observed in the (Sc/Ta)2.0 ceramic, as oxygen ions and $V_O^{\cdot\cdot}$ diffusion contributes to grain growth.[40]

Fig. 6 presents the frequency dependence of ε' and tan δ at 25 °C for the ScTa-TO ceramics with different Sc^{3+}/Ta^{5+} ratios. The ε' and tan δ values exhibit distinct trends across the frequency range (40–10^6 Hz), depending on the Sc^{3+} concentration or Sc^{3+}/Ta^{5+} ratios. As shown in Fig. 6a, the ceramics with Sc^{3+}/Ta^{5+} ratios of 0.4, 0.8, and 1.0 exhibit exceptionally high ε' values (>10^4), consistent with previous studies on various co-doped TiO_2 systems. In contrast, the (Sc/Ta)1.2, (Sc/Ta)1.6, and (Sc/Ta)2.0 ceramics do not display a giant dielectric response, despite containing the same Ta^{5+} concentration as the other compositions. Notably, its ε' value is on the order of 10^2, comparable to that of pure rutile TiO_2,[7] which is primarily attributed to ionic polarization. Furthermore, the ε' value of the (Sc/Ta)1.0 ceramic is not the highest among the compositions. If there were no interaction between Sc^{3+} and Ta^{5+}, ε' should remain unchanged across all ceramics, as Ta^{5+}—the primary source of free electrons—is present at the same concentration in each sample. Table 2 summarizes the ε' and tan δ values at 25 °C and 1 kHz for all ceramics, where a clear trend is observed: ε' decreases with increasing Sc^{3+}/Ta^{5+} ratio, despite the consistent Ta^{5+} doping level. This behavior is similar to that reported

Table 2 Dielectric properties at 1 kHz and activation energy of ScTa-TO ceramics with Sc^{3+}/Ta^{5+} ratios of 0.4, 0.8, 1.0, and 2.0

Sample	Dielectric properties		Temperature range of $\Delta\varepsilon'(T)/\varepsilon'_{25} \leq \pm 15\%$	E_a (eV)
	ε' (25 °C)	Tan δ (25 °C)		
(Sc/Ta)0.4	5.94×10^4	0.024	−60–200 °C	∼0.831
(Sc/Ta)0.8	4.81×10^4	0.043	−60–200 °C	∼1.214
(Sc/Ta)1.0	2.05×10^4	0.070	−40–190 °C	∼1.246
(Sc/Ta)1.2	1.46×10^2	0.060	—	—
(Sc/Ta)1.6	1.92×10^2	0.058	—	—
(Sc/Ta)2.0	1.55×10^2	0.040	—	—

for AlNb-TO ceramics.[28] Based on the IBLC model,[3] the observed reduction in ε' may be attributed to an increase in grain boundary thickness or a decrease in free charge carriers within semiconducting grains. Although grain boundary thickness measurements require TEM analysis, it is evident that the decrease in ε' correlates with the increasing Sc^{3+}/Ta^{5+} ratio. Theoretically, ε' should depend solely on the Ta^{5+} concentration, but these results suggest that Sc^{3+} also plays a role, likely by influencing the availability of free charge carriers. Although the (Sc/Ta)0.4 and (Sc/Ta)0.8 ceramics exhibit higher ε' values than the (Sc/Ta)1.0 ceramic, it is premature to conclude that they possess optimized dielectric properties.

Fig. 6b shows the variation of tan δ with frequency at 25 °C for the ScTa-TO ceramics. At low frequencies (<10^4 Hz), tan δ remains relatively low for all compositions. As summarized in Table 2, the (Sc/Ta)1.0 ceramic exhibits the highest tan δ, further indicating that the Sc^{3+}/Ta^{5+} ratio of 1.0 is not optimal. This trend is consistent with our previous findings for the same composition sintered at 1500 °C with Au-sputtered electrodes, where the dielectric properties were also not optimized despite using a 1 : 1 ratio.[33] The sharp increase in tan δ at higher frequencies suggests the presence of a dielectric relaxation mechanism,[3,14,24] similar to those observed in other giant dielectric materials such as $CaCu_3Ti_4O_{12}$ (CCTO),[41] CuO,[6] and NiO.[3] The relatively low tan δ observed in the (Sc/Ta)0.4 and (Sc/Ta)0.8 ceramics indicate their potential suitability for high-performance capacitor applications.

Beyond achieving a high ε' and low tan δ, the temperature dependence of ε' is a crucial factor in determining the suitability of dielectric materials for ceramic applications.[42] To assess thermal stability, ε' was thoroughly investigated for the (Sc/Ta)0.4, (Sc/Ta)0.8, and (Sc/Ta)1.0 ceramics, all of which exhibit giant ε' values exceeding 10^4. As shown in Fig. 7, ε' remains exceptionally stable over a broad temperature range from −180 to 210 °C at 1 kHz. The inset of Fig. 7 reveals that tan δ remains below 0.1 between −60 and 200 °C, with the (Sc/Ta)0.4 and (Sc/Ta)0.8 ceramics exhibiting lower tan δ values than (Sc/Ta)1.0 within this range.

To further quantify the thermal stability of ε', the temperature coefficient $\Delta\varepsilon'(T)/\varepsilon'_{25}$ (where ε'_{25} represents ε' at 25 °C) was

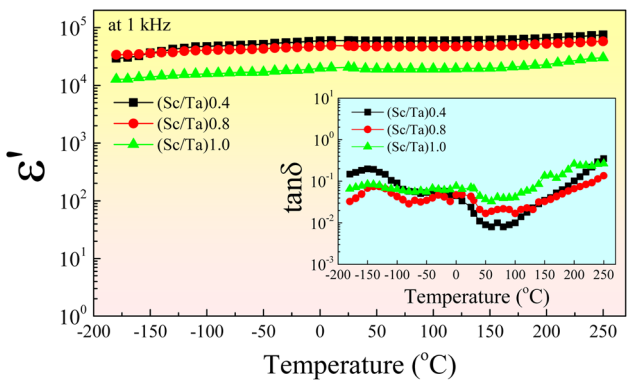

Fig. 7 Temperature dependence of ε' at 1 kHz for ScTa-TO ceramics with Sc^{3+}/Ta^{5+} ratios of 0.4, 0.8, and 1.0; inset shows tan δ at 1 kHz.

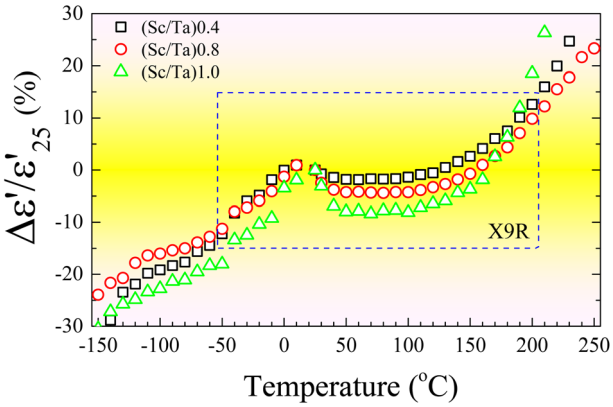

Fig. 8 Temperature coefficient of ε' at 1 kHz for ScTa-TO ceramics with Sc^{3+}/Ta^{5+} ratios of 0.4, 0.8, and 1.0.

calculated for all compositions. As illustrated in Fig. 8, the (Sc/Ta)0.4 and (Sc/Ta)0.8 ceramics exhibit excellent stability, with fluctuations within ±15% over the entire range of −60 to 200 °C. In contrast, the (Sc/Ta)1.0 ceramic shows more pronounced variations, indicating a less stable dielectric response at higher Sc^{3+} doping levels. The remarkable thermal stability observed in (Sc/Ta)0.4 and (Sc/Ta)0.8 ceramics is particularly notable when compared to other giant dielectric materials, such as CCTO, CuO, NiO-based oxides, $La_{2-x}Sr_xNiO_4$, and $AFe_{1/2}B_{1/2}O_3$ (B = Nb and Ta) compounds.[3,6,41,43,44] These comparisons highlight the superior temperature performance of (Sc/Ta)0.4 and (Sc/Ta)0.8, making them promising candidates for applications requiring highly stable dielectric properties in fluctuating thermal environments. This stability likely arises from a combination of intrinsic factors, such as charge compensation between Sc^{3+} and Ta^{5+} ions, and extrinsic effects related to grain boundary characteristics.

The (Sc/Ta)0.4 and (Sc/Ta)0.8 ceramics likely exhibit the most stable dielectric behavior, characterized by low tan δ and consistent ε' values across a wide temperature range. This superior dielectric performance is attributed to a well-balanced interaction between interfacial polarization and the electrical properties of both grains and grain boundaries. These findings emphasize the critical role of Sc^{3+}/Ta^{5+} ratio in tuning the dielectric properties of ScTa-TO ceramics. Interestingly, the optimal dielectric performance was not observed in the (Sc/Ta)1.0 ceramic, where the Sc^{3+}/Ta^{5+} ratio is 1.0, a condition commonly reported in other co-doped systems such as InTa-TO and InNb-TO.[8,32] This suggests that the optimal dielectric properties may not necessarily be achieved at a +3/+5 ion ratio of 1.0, a phenomenon that remains underexplored in existing literature. In contrast, studies on $Al_xNb_{0.03}Ti_{0.97-x}O_2$ ceramics indicate that the best dielectric properties were still obtained at $x = 0.03$ (Al^{3+}/Nb^{5+} ratio = 1.0).[28]

Typically, the enhancement of dielectric properties in TiO_2 ceramics is attributed to the incorporation of Ta^{5+} into the rutile TiO_2 matrix, which generates free electrons through the following reactions:[9,16,18,32]

$$2TiO_2 + Ta_2O_5 \xrightarrow{4TiO_2} 2Ti'_{Ti} + 2Ta^{\cdot}_{Ti} + 8O_O + 1/2O_2 \quad (2)$$

$$Ti^{4+} + e \rightarrow Ti^{3+} \quad (3)$$

The introduction of Ta^{5+} results in a high ε' due to the generation of free electrons; however, it also leads to an increased tan δ.[14] The observed reduction in tan δ is attributed to the substitution of Sc^{3+} ions. Based on eqn (2) and (3), the dielectric response of all ScTa-TO ceramics should, in theory, remain similar, as ε' is primarily governed by the donor (Ta^{5+}) concentration, which is consistent across all samples. However, experimental results indicate that ε' decreases with increasing Sc^{3+} concentration. This decline in dielectric response cannot be attributed to grain size variations, as the average grain size increases with higher Sc^{3+} doping levels. Instead, the observed reduction in ε' is likely associated with extrinsic factors, particularly the electrical properties of grains and grain boundaries, which will be discussed in subsequent sections.

To further elucidate the origin of the giant dielectric response in the (Sc/Ta)0.4, (Sc/Ta)0.8, and (Sc/Ta)1.0 ceramics and to clarify the influence of the Sc^{3+}/Ta^{5+} ratio on dielectric properties, impedance spectroscopy was used to investigate the electrical characteristics of grains and grain boundaries. As shown in Fig. 9a, all three compositions exhibit a nonzero intercept on the Z' axis at 25 °C, confirming the presence of semiconducting grains,[5,9,14] which is due to Ta^{5+} doping (as described in eqn (2) and (3)) and insulating grain boundaries formed by Sc^{3+} doping. In contrast, the (Sc/Ta)2.0 ceramic shows no intercept on the Z' axis, indicating the absence of semiconducting grains and, consequently, the lack of an IBLC structure—which is consistent with its low ε'. In conventional $BaTiO_3$-based ceramics, the formation of IBLC structures typically requires complex processing procedures, including high-temperature sintering under carefully controlled reducing atmospheres, followed by partial reoxidation to form thin insulating grain boundary layers.[45] In contrast, the ScTa-TO ceramics examined in this study successfully develop a stable IBLC structure through a much simpler route—sintering in ambient air. This approach is similar to that used for CCTO-based materials but offers better control over tan δ. The formation of the IBLC structure in ScTa-TO ceramics is attributed to the deliberate tuning of acceptor and donor dopant concentrations, eliminating the need for strict atmosphere control during processing.

Fig. S4† and its inset provide additional evidence supporting the IBLC effect. At 25 °C, the insulating grain boundary arc is not fully resolved, and only a partial semicircular arc is visible in all ceramics. However, the presence of these partial arcs strongly suggests that these ceramics are electrically heterogeneous, consisting of semiconducting grains and insulating grain boundaries. Furthermore, the nonzero intercept on the Z' axis increases with the Sc^{3+}/Ta^{5+} ratio, indicating a corresponding increase in grain resistance (R_g).[5] This trend culminates in the (Sc/Ta)2.0 ceramic, where no semiconducting grains are present, leading to a complete suppression of the IBLC effect. The increase in R_g with higher Sc^{3+} content can be attributed to self-charge compensation between Sc^{3+} and Ta^{5+}, following the reaction:

$$Sc_2O_3 + 2TiO_2 + Nb_2O_5 \xrightarrow{6TiO_2} 2Sc'_{Ti} + 2Nb^{\bullet}_{Ti} + 2Ti_{Ti} + 12O_O \quad (4)$$

The absence of the IBLC effect in (Sc/Ta)2.0 suggests that excessive Sc^{3+} doping promotes self-charge compensation, eliminating the formation of semiconducting grains due to the absence of free electrons (as described in eqn (2) and (3)), thereby significantly reducing the ε'. This supports the hypothesis that an optimal balance between donor (Ta^{5+}) and acceptor (Sc^{3+}) concentrations is essential for maintaining the IBLC structure and maximizing the dielectric response. Even at the highest measured temperature (*i.e.*, 250 °C), none of the (Sc/Ta)0.4, (Sc/Ta)0.8, or (Sc/Ta)1.0 ceramics exhibit a fully developed semicircle, as shown in the inset of Fig. 9b. However, the persistence of partial semicircular arcs at higher temperatures further confirms that their giant dielectric response originates from interfacial polarization at the boundaries between semiconducting grains and insulating grain layers, consistent with the IBLC mechanism.[3,5,9,41] The inability to fully resolve the grain boundary response at elevated temperatures suggests that the insulating grain boundaries retain high resistance (R_{gb}). Furthermore, a strong correlation between the ε' value and the electrical properties of the semiconducting grains can be

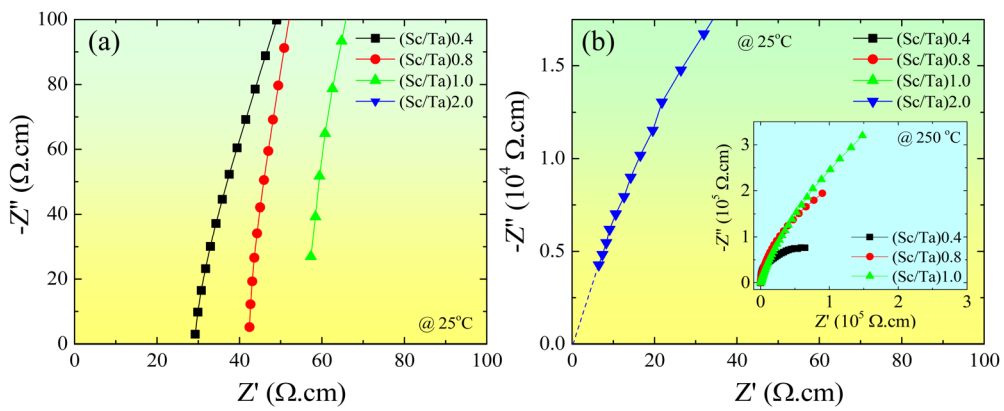

Fig. 9 (a) Impedance complex plane (Z^*) plots at 25 °C for (Sc/Ta)0.4, (Sc/Ta)0.8, and (Sc/Ta)1.0 ceramics. (b) Z^* plot of (Sc/Ta)2.0 ceramic at 25 °C; inset shows Z^* plots at 250 °C for (Sc/Ta)0.4, (Sc/Ta)0.8, (Sc/Ta)1.0 ceramics.

established. The observed increase in R_g directly indicates a reduction in free charge concentration within the semiconducting grains. Under an applied electric field, as the free charge concentration decreases, the accumulated charges at the grain boundaries are reduced, weakening interfacial polarization and consequently lowering the ε' value as the Sc^{3+}/Ta^{5+} ratio increases. This behavior closely resembles that observed in Li and Ti co-doped NiO, where the dielectric response declines with decreasing free charge concentration in the semiconducting grains due to the reduced Li^+ doping levels.[3]

To further investigate the influence of the Sc^{3+}/Ta^{5+} ratio on the electrical properties of semiconducting grains, XPS was employed to analyze the valence states of Ti in the ScTa-TO ceramics. As shown in Fig. 10, the Ti 2p spectra of (Sc/Ta)0.4, (Sc/Ta)1.0, and (Sc/Ta)2.0 exhibit characteristic Ti $2p_{3/2}$ and Ti $2p_{1/2}$ peaks at 458.4 eV and 464.2 eV, respectively, which are indicative of Ti^{4+}.[8,16,22] Spectral deconvolution, performed using a combination of Gaussian and Lorentzian functions, revealed the presence of Ti^{3+} at ~457.3 eV[8, 22] in the (Sc/Ta)0.4 and (Sc/Ta)1.0 ceramics. In contrast, no Ti^{3+} signal was detected in the (Sc/Ta)2.0 ceramic, confirming that only Ti^{4+} is present in this composition. Quantitative analysis further showed that the Ti^{3+}/Ti^{4+} ratios in (Sc/Ta)0.4 and (Sc/Ta)1.0 were 2.34% and 1.78%, respectively, indicating a partially reduced Ti state. This reduction is associated with free-electron generation, which facilitates the formation of semiconducting grains. These findings correlate with the R_g trends observed in Fig. 9a, as the Ti^{3+}/Ti^{4+} ratio decreases, R_g increases, suggesting a lower concentration of charge carriers. Notably, the (Sc/Ta)2.0 ceramic exhibits neither Ti^{3+} nor a nonzero intercept in the impedance spectrum, confirming the absence of semiconducting grains. The dominance of Ti^{4+} in the (Sc/Ta)2.0 ceramic supports the hypothesis that excessive Sc^{3+} doping promotes self-charge compensation, effectively suppressing free-electron generation and eliminating the IBLC effect. The XPS analysis provides direct evidence that variations in the Sc^{3+}/Ta^{5+} ratio influence the reduction state of Ti, which in turn governs the formation of semiconducting grains. A higher concentration of Ti^{3+} promotes free-electron availability, leading to lower R_g, which enhances interfacial polarization and giant dielectric behavior.

To further investigate the influence of the Sc^{3+}/Ta^{5+} ratio on the electrical properties of insulating grain boundaries, impedance spectroscopy was used to analyze their R_{gb} values. Although a fully developed semicircular arc, which represents the electrical response of insulating grain boundaries,[5] was not observed even at the highest measured temperature (250 °C), the onset of curvature was detected at 210 °C. This indicates the initial formation of a discernible grain boundary response at elevated temperatures. To estimate R_{gb}, the impedance data were fitted using the following equation[4]

$$Z^* = \frac{R_{gb}}{1 + (i\omega R_{gb} C_{gb})^{\beta}} \quad (5)$$

where β is a constant ($0 < \beta \leq 1$), i is the imaginary unit ($\sqrt{-1}$), C_{gb} represents the grain boundary capacitance, and ω is the angular frequency of the applied electric field. As shown in Fig. 11a, the Z^* plots of the (Sc/Ta)0.8 ceramic in the 210–250 °C range were well fitted using eqn (5). Similar fitting was successfully applied to the (Sc/Ta)0.4 and (Sc/Ta)1.0 ceramics, enabling the determination of R_{gb} values at different temperatures. The temperature dependence of R_{gb} was further analyzed using the Arrhenius equation:

$$R_{gb} = R_0 \exp\left(\frac{E_{gb}}{k_B T}\right) \quad (6)$$

where T is the absolute temperature (K), k_B is the Boltzmann constant, R_0 is a pre-exponential factor, and E_{gb} represents the activation energy required for conduction across the insulating grain boundary. As shown in Fig. 11b, the linear fits yielded E_{gb} values for the (Sc/Ta)0.4, (Sc/Ta)0.8, and (Sc/Ta)1.0 ceramics in the range of 0.831–1.246 eV. The E_{gb} values increased with increasing the Sc^{3+}/Ta^{5+} ratio. These values, which are summarized in Table 2, are directly related to the electrostatic potential barrier height (Φ_b) at the grain boundaries. Notably, the E_{gb} (or Φ_b) values in these ceramics are significantly higher than those reported for CCTO and related materials.[4,5,41] The presence of such high potential barriers effectively suppresses charge carrier conduction across grain boundaries, thereby minimizing dielectric losses. Consequently, the low tan δ observed in these ceramics can be attributed to the high electrostatic potential barrier (Schottky barrier) at the grain

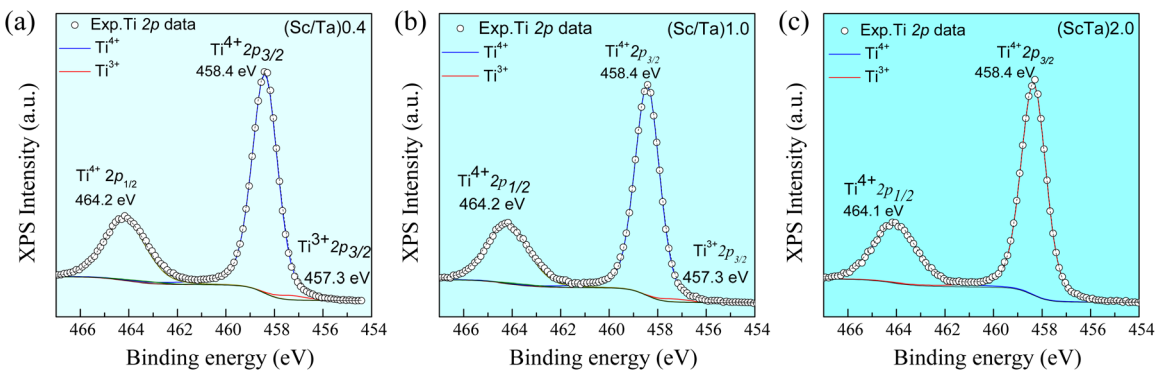

Fig. 10 XPS spectra of Ti 2p for ScTa-TO ceramics with Sc^{3+}/Ta^{5+} ratios of (a) 0.4, (b) 1.0, and (c) 2.0.

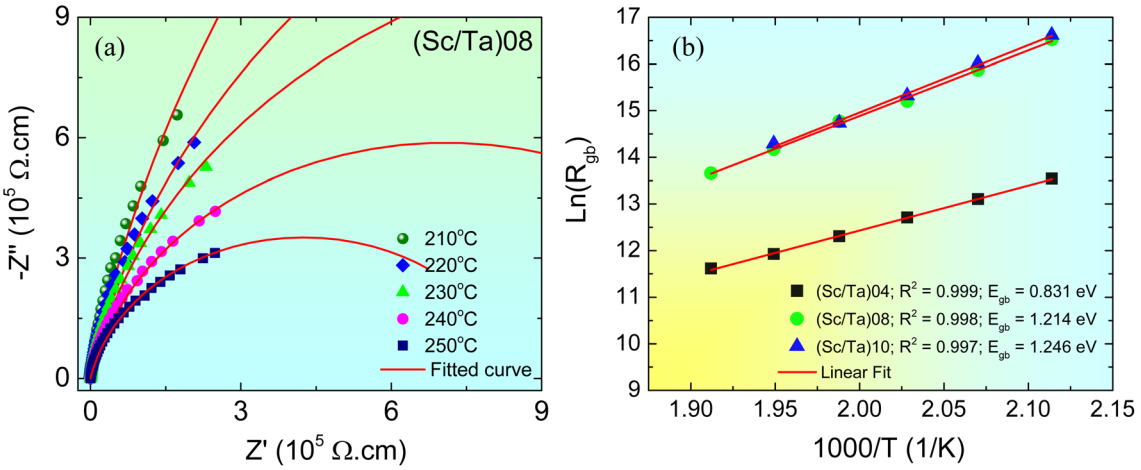

Fig. 11 (a) Z^* plots of (Sc/Ta)0.8 ceramic at different temperatures from 210 to 250 °C fitted by eqn (5). (b) Arrhenius plots of temperature dependence of R_{gb} for (Sc/Ta)0.4, (Sc/Ta)0.8, and (Sc/Ta)1.0 ceramics.

boundaries, which plays a crucial role in maintaining excellent dielectric stability.

The J–E characteristics of the ScTa-TO ceramics with different Sc^{3+}/Ta^{5+} ratios are displayed in Fig. 12, further confirming the existence of Schottky barriers at the grain boundaries in the (Sc/Ta)0.4, (Sc/Ta)0.8, and (Sc/Ta)1.0 ceramics. These ceramics exhibited a distinct nonlinear J–E response, while the (Sc/Ta)2.0 ceramic displayed purely ohmic behavior, consistent with the absence of semiconducting grains observed in impedance spectroscopy (Fig. 9). For the (Sc/Ta)0.4, (Sc/Ta)0.8, and (Sc/Ta)1.0 ceramics, the nonlinearity in J–E curves with α values in the range of 1.5 to 2.0 arises from the potential barrier at the grain boundaries, supporting the IBLC model as the dominant mechanism governing the dielectric properties of these materials. It is worth noting that the α values observed in this study are consistent with those of surface-polished samples reported in our previous work on 2.5% ($Sc_{1/2}Ta_{1/2}$) co-doped TiO_2.[9] In that study, α dropped significantly from ~37 (as-fired) to ~2.6 after polishing, confirming that the SBLC effect was effectively removed. This validates that the dielectric behavior observed here is primarily governed by the IBLC mechanism.

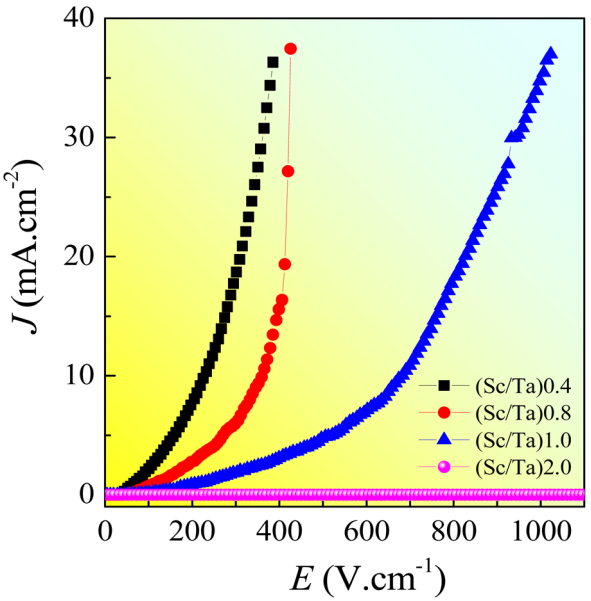

Fig. 12 Nonlinear J–E characteristics of all ScTa-TO ceramics with different Sc^{3+}/Ta^{5+} ratios.

The nonzero intercepts in the impedance spectra and the observed nonlinear J–E behavior collectively demonstrate that these compositions possess electrically heterogeneous structures, consisting of semiconducting grains and insulating grain boundaries. In contrast, the (Sc/Ta)2.0 ceramic lacks a nonlinear J–E response due to absence of semiconducting grains in this sample, which suggests that excessive Sc^{3+} doping promotes self-charge compensation, reducing the availability of free electrons and preventing the formation of an IBLC structure. Consequently, the (Sc/Ta)2.0 ceramic does not exhibit giant dielectric properties, further confirming that the interfacial polarization effect at the grain boundaries is critical to the observed high ε' in the (Sc/Ta)0.4, (Sc/Ta)0.8, and (Sc/Ta)1.0 ceramics. The E_b values of the (Sc/Ta)0.4, (Sc/Ta)0.8, and (Sc/Ta)1.0 ceramics were determined to be 66, 117, and 214 V cm^{-1}, respectively. These values correlate well with the E_{gb} and R_{gb} observed in the Arrhenius plots, Fig. 11b. Although these relatively low breakdown fields may limit their applicability in high-voltage devices, the combination of high ε', low tan δ, and excellent temperature stability makes these ceramics promising candidates for embedded capacitors and low-power electronic components. Moreover, the chemical stability of the TiO_2 matrix and the thermal robustness of the Sc^{3+} and Ta^{5+} dopants suggest good long-term reliability. The ability to achieve IBLC structures through air sintering further enhances their compatibility with scalable and cost-effective fabrication processes. However, due to the extrinsic nature of the dielectric response, which relies on grain boundary effects, these materials may not be suitable for applications requiring thin films,

multilayer architectures, or dielectric composites, where the formation of IBLC structures is typically constrained.

Taken together, the combination of surface polishing to suppress SBLC contributions, the observed electrical heterogeneity from impedance analysis, the nonlinear *J–E* characteristics associated with Schottky-type grain boundary barriers, and the absence of EPDD-related defects strongly confirms that the dielectric response in ScTa-TO ceramics[9] is primarily governed by the IBLC mechanism. It should be noted that no secondary phases or abnormal structural distortions were detected in the XRD and Raman spectra, suggesting that extrinsic factors such as impurities or local structural defects have negligible influence on the dielectric response in these ceramics.

By challenging the conventional assumption that a 1 : 1 acceptor/donor ratio is necessary for optimal performance in co-doped TiO_2 ceramics, this work demonstrates a new strategy for achieving enhanced dielectric properties—characterized by high ε', low tan δ, and excellent temperature stability. Unlike our previous study, which focused primarily on humidity sensing performance and observed only moderate dielectric values,[33] the present work systematically tunes the Sc^{3+}/Ta^{5+} ratio and establishes a clear relationship between doping ratio, microstructure, and dielectric response. These insights provide a more comprehensive understanding of defect control and interfacial polarization mechanisms in IBLC-dominated systems. Beyond its fundamental contributions, this study offers a broadly applicable framework for designing high-permittivity ceramics, with implications for capacitors, energy storage devices, and advanced dielectric materials through precise control of defect chemistry and microstructural engineering. This approach is particularly well suited for co-doped TiO_2 systems where the dielectric response is governed primarily by extrinsic mechanisms, such as interfacial polarization *via* IBLC, and where EPDD-related effects are negligible or absent. In such systems, tuning the acceptor/donor ratio provides a powerful strategy to enhance dielectric properties without relying on complex defect dipole formation.

4. Conclusions

We investigated how the acceptor/donor doping ratio influenced the microstructure and giant dielectric behavior of co-substituted TiO_2 ceramics. Specifically, we synthesized Sc_x-$Ta_{0.025}Ti_{0.975-x}O_2$ ceramics, with Sc^{3+}/Ta^{5+} ratios of 0.4, 0.8, 1.0, and 2.0, *via* SSR method. All samples exhibited a dense rutile TiO_2 phase. Raman spectroscopy revealed that increasing the Sc^{3+}/Ta^{5+} ratio led to the formation of $V_O^{\cdot\cdot}$, which in turn resulted in larger average grain sizes. As this ratio increased, the ε' dropped markedly, and no giant dielectric response was observed for ratios above 1.0. By contrast, ratios of 0.4 and 0.8 yielded high ε' values of 5.9×10^4 and 4.8×10^4, respectively, along with low tan δ values of 0.024 and 0.043 at 1 kHz and 25 °C. These ceramics also retained stable dielectric characteristics over a broad temperature range (−60 to 210 °C), with variations less than ±15%, thereby satisfying the X9R capacitor standard. Impedance spectroscopy and nonlinear electrical measurements confirmed that the enhanced dielectric performance was primarily governed by interfacial polarization between semiconducting grains and insulating grain boundaries, supported by XPS analysis. Notably, the optimal dielectric response commonly associated with an acceptor/donor ratio of 1.0 in other co-doped systems was not observed in this work, emphasizing the importance of tailoring the doping ratio based on the dominant mechanism involved. These findings demonstrate that the ideal acceptor/donor ratio is not universal across all co-doped TiO_2 ceramics but is instead dependent on the primary dielectric mechanism. While a 1 : 1 ratio may be essential for systems driven by EPDD, our results show that lower ratios can be more effective in IBLC-dominated systems by reducing self-compensation and maintaining semiconducting grain behavior. This approach offers a useful framework for optimizing extrinsically governed co-doped TiO_2 ceramics.

Data availability

All data are included in the manuscript. The data supporting this article have been included as part of the ESI.†

Author contributions

Wattana Tuichai; conceptualization, methodology, validation, data curation, formal analysis, investigation, visualization. Jurimart Wongsricha; methodology, investigation. Nutthakritta Phromviyo; methodology, investigation. Bundit Putasaeng; methodology, resources. Supamas Danwittayakul; conceptualization, resources, funding acquisition. Pornjuk Srepusharawoot; software, formal analysis. Prasit Thongbai; conceptualization, methodology, validation, formal analysis, investigation, resources, writing – original draft, writing – review & editing, visualization, supervision, project administration, funding acquisition.

Conflicts of interest

There are no conflicts to declare.

Acknowledgements

This research was supported by the Fundamental Fund of Khon Kaen University and the National Science, Research, and Innovation Fund (NSRF). Additional support was provided by the Research of Khon Kaen University. W. Tuichai would like to thank the Thailand Graduate Institute of Science and Technology (TGIST) for his PhD scholarship.

References

1 L. Yang, H. Wang, F. Zhang, Y. Yang, S. Qu, D. Leng and X. Ma, *Nano Energy*, 2023, **114**, 108609.
2 Y. Wang, W. Jie, C. Yang, X. Wei and J. Hao, *Adv. Funct. Mater.*, 2019, **29**, 1808118.
3 J. Wu, C.-W. Nan, Y. Lin and Y. Deng, *Phys. Rev. Lett.*, 2002, **89**, 217601.

4 J. Liu, C.-G. Duan, W.-G. Yin, W. Mei, R. Smith and J. Hardy, *Phys. Rev. B:Condens. Matter Mater. Phys.*, 2004, **70**, 144106.
5 T. Adams, D. Sinclair and A. West, *Phys. Rev. B:Condens. Matter Mater. Phys.*, 2006, **73**, 094124.
6 S. Sarkar, P. K. Jana, B. K. Chaudhuri and H. Sakata, *Appl. Phys. Lett.*, 2006, **89**, 212905.
7 C. C. Homes and T. Vogt, *Nat. Mater.*, 2013, **12**, 782–783.
8 W. Hu, Y. Liu, R. L. Withers, T. J. Frankcombe, L. Norén, A. Snashall, M. Kitchin, P. Smith, B. Gong, H. Chen, J. Schiemer, F. Brink and J. Wong-Leung, *Nat. Mater.*, 2013, **12**, 821–826.
9 W. Tuichai, P. Srepusharawoot, S. Danwittayakul and P. Thongbai, *Sci. Rep.*, 2024, **14**, 2593.
10 W. C. Ribeiro, E. Joanni, R. Savu and P. R. Bueno, *Solid State Commun.*, 2011, **151**, 173–176.
11 W. Dong, W. Hu, A. Berlie, K. Lau, H. Chen, R. L. Withers and Y. Liu, *ACS Appl. Mater. Interfaces*, 2015, **7**, 25321–25325.
12 P. Lunkenheimer, R. Fichtl, S. Ebbinghaus and A. Loidl, *Phys. Rev. B:Condens. Matter Mater. Phys.*, 2004, **70**, 172102.
13 M. Li, A. Feteira and D. C. Sinclair, *J. Appl. Phys.*, 2009, **105**, 114109.
14 W. Tuichai, S. Danwittayakul, N. Chanlek and P. Thongbai, *Mater. Res. Bull.*, 2019, **116**, 137–142.
15 W. Tuichai, S. Danwittayakul, N. Chanlek, P. Thongbai and S. Maensiri, *J. Alloys Compd.*, 2017, **703**, 139–147.
16 W. Tuichai, N. Thongyong, S. Danwittayakul, N. Chanlek, P. Srepusharawoot, P. Thongbai and S. Maensiri, *Mater. Des.*, 2017, **123**, 15–23.
17 J. Li, F. Li, C. Li, G. Yang, Z. Xu and S. Zhang, *Sci. Rep.*, 2015, **5**, 8295.
18 N. Thongyong, K. Sreejivungsa, P. Kawee, N. Chanlek, M. Takesada and P. Thongbai, *J. Alloys Compd.*, 2024, **989**, 174341.
19 N. Thongyong, N. Chanlek, P. Srepusharawoot, M. Takesada, D. P. Cann and P. Thongbai, *J. Eur. Ceram. Soc.*, 2022, **42**, 4944–4952.
20 J. Fan, G. He, Z. Cao, Y. Cao, Z. Long and H. Zhanggui, *J Materiomics*, 2023, **9**, 157–165.
21 P. Qiao, Y. Zhang, J. Wang, Z. Peng, D. Wu, X. Chao, Z. Yang and P. Liang, *Ceram. Int.*, 2024, **50**, 2242–2248.
22 Y. Xue, Z. Wang, Y. Li, Z. Yi, X. Li and D. Wu, *J. Mater. Sci.: Mater. Electron.*, 2023, **34**, 864.
23 J.-J. Ma, Y. Gao, Y. Chen and M.-H. Wang, *J. Electron. Mater.*, 2023, **52**, 3698–3705.
24 J. Fan, Z. Long, H. Zhou, G. He and Z. Hu, *J. Alloys Compd.*, 2022, **921**, 166200.
25 H. Zhang, X. Huang, X. Liao and D. Zhu, *Mater. Sci. Semicond. Process.*, 2023, **163**, 107568.
26 T. Yang and J. Liang, *J. Alloys Compd.*, 2022, **929**, 167323.
27 Y. Mingmuang, N. Chanlek and P. Thongbai, *J Materiomics*, 2022, **8**, 1269–1277.
28 Y. Song, X. Wang, X. Zhang, Y. Sui, Y. Zhang, Z. Liu, Z. Lv, Y. Wang, P. Xu and B. Song, *J. Mater. Chem. C*, 2016, **4**, 6798–6805.
29 L. Zhou, Z. Peng, M. Jiang, G. Yang, H. Liu, D. Wu, P. Liang, L. Wei, X. Chao and Z. Yang, *Ceram. Int.*, 2024, **50**, 3252–3259.
30 L. Zhou, Z. Peng, J. Zhu, Q. Shi, P. Liang, L. Wei, D. Wu, X. Chao and Z. Yang, *Mater. Chem. Phys.*, 2023, **295**, 127072.
31 Z. Yang, X. Wang, L. Zhang, H. Li, H. Zhang and D. Xu, *Ceram. Int.*, 2024, **50**(11), 18993–19001.
32 W. Dong, W. Hu, T. J. Frankcombe, D. Chen, C. Zhou, Z. Fu, L. Candido, G. Hai, H. Chen, Y. Li, R. L. Withers and Y. Liu, *J. Mater. Chem. A*, 2017, **5**, 5436–5441.
33 K. Phuion, W. Tuichai, J. Wongsricha, K. Sreejivungsa, N. Thanamoon, N. Phromviyo, W. Jarernboon and P. Thongbai, *J. Alloys Compd.*, 2025, **1010**, 177639.
34 W. Hao, P. Xu, L. Sun and E. Cao, *Ceram. Int.*, 2023, **49**, 40650–40658.
35 A. J. Atanacio, M. A. Alim, T. Bak, M. Ionescu and J. Nowotny, *J. Am. Ceram. Soc.*, 2017, **100**, 419–428.
36 W. Hu, K. Lau, Y. Liu, R. L. Withers, H. Chen, L. Fu, B. Gong and W. Hutchison, *Chem. Mater.*, 2015, **27**, 4934–4942.
37 G. Liu, H. Fan, J. Xu, Z. Liu and Y. Zhao, *RSC Adv.*, 2016, **6**, 48708–48714.
38 L. Wang, J. Li, X. Liu, M. Zhang, X. Li, S. Liu and X. Sun, *Ceram. Int.*, 2023, **49**, 32116–32126.
39 J. C. Parker and R. W. Siegel, *Appl. Phys. Lett.*, 1990, **57**, 943–945.
40 M. N. Rahaman, *Ceramic Processing and Sintering*, M. Dekker, New York, 2nd edn, 2003.
41 L. M. Jesus, L. B. Barbosa, D. R. Ardila, R. S. Silva and J. C. M'Peko, *Ceram. Int.*, 2023, **49**, 25594–25601.
42 M. Pan and C. A. Randall, *IEEE Electr. Insul. Mag.*, 2010, **26**, 44–50.
43 X. Q. Liu, G. Liu, P. P. Ma, G. J. Li, J. W. Wu and X. M. Chen, *J. Electroceram.*, 2016, **37**, 73–78.
44 M. Amara, J. Hellara, J. Laifi, F. Bourguiba, J. Dhahri, K. Khirouni and E. K. Hlil, *J. Inorg. Organomet. Polym. Mater.*, 2024, **34**, 664–679.
45 D. C. Sinclair, T. B. Adams, F. D. Morrison and A. R. West, *Appl. Phys. Lett.*, 2002, **80**, 2153.